Restoring erythromycin efficacy by the repurposed drugs desloratadine and zinc gluconate as adjuvants via bacterial efflux pump inhibition

Rukunuzzaman Mia
University of Rajshahi
Chandan Barai
University of Rajshahi
Rafat Hossain Rafi
University of Rajshahi
Anamul Haque
University of Rajshahi
Md. Abdul Alim Al-Bari
alimalbari347@ru.ac.bd

University of Rajshahi

Article

Keywords: Antibiotic resistance, adjuvant therapy, efflux pump inhibitor, lung histopathology, in silico study, MM/PBSA analysis

Posted Date: July 9th, 2026

DOI: https://doi.org/10.21203/rs.3.rs-9956217/v1

Additional Declarations: No competing interests reported.

Abstract

Antibiotic resistance is progressively threatening our global health and impeding the management of infectious diseases. Efflux pump overexpression is one of the mechanisms that contribute to bacterial biofilm formation, thereby synergistically driving antibiotic resistance. However, to address it, antibiotic adjuvants, as efflux pump inhibitors (EPIs), are potential candidates to inhibit bacterial biofilms and restore obsolete antibiotics' effectiveness, thereby reducing research and development expenditures. Our findings demonstrated that desloratadine and zinc gluconate as adjuvants exhibited synergism with erythromycin against *Escherichia coli* ATCC-25922, *Acinetobacter baumannii* NCTC-12156, *Pseudomonas aeruginosa* ATCC-27853, and *Staphylococcus aureus* ATCC-25923 via in vitro combined susceptibility assays, including disk diffusion and a resazurin-based turbidimetric test. Alongside these, evaluated clinical parameters including total white blood cell (WBC) count, percentage of body weight changes, lung weight index, and lung histopathology demonstrated that the erythromycin-desloratadine and erythromycin-zinc gluconate combination boosted clinical efficacy in an in vivo mouse model via reducing lung inflammation and restoring more intact alveolar cells. Afterward, to investigate EPIs, molecular docking, MM/PBSA, and molecular dynamic (MD) simulation over 100 ns were performed for both adjuvants with the targeted efflux protein, AbeJ of *A. baumannii* NCTC-12156, where favorable binding affinities, binding free energies (△G), and stable conformations during analyses support the conclusion that both adjuvants inhibited the efflux pump and restored erythromycin efficacy.

Introduction

The emergence of multidrug-resistant (MDR) pathogens, fueled by antimicrobial resistance (AMR), endangers effective treatment for infectious diseases and leads to approximately 9% of global mortality.[1] Experts' assessment suggests that AMR could result in major health and economic impacts by 2030, propelling 2.4 crore population into extreme poverty, especially in low and middle-income countries (LMICs).[1, 2] If current trends continue, the mortality rate of AMR is projected to elevate, causing roughly 1.91 million fatalities directly ascribable and 8.22 million fatalities linked with AMR by 2050.[3] The current Global Antibiotic Resistance Surveillance Report 2025 addresses eight prevalent bacteria, including Gram-negative bacteria (*Acinetobacter spp.*, *E. coli*, *K. pneumoniae*, *N. gonorrhoeae*, non-typhoidal *Salmonella spp.*, and *Shigella spp.*), and Gram-positive bacteria (Methicillin-resistant *S. aureus* (MRSA) and *S. pneumoniae*), which are resistant to 22 antibiotics used to treat various infectious diseases like UTIs, GI infections, septicemia, and gonorrhoeae.[4] David Brown et al. reported that Gram-negative bacteria predominantly exhibit higher resistance, with specific cases indicating resistance rates reaching up to 50% against carbapenems, which are currently considered the last line of defense in certain developing countries.[5]

Unlike most critical, *Acinetobacter baumannii* and other MDR Gram-negative bacteria frequently become prevalent via the overexpression of the transporters RND (Resistance-nodulation-cell division) superfamily, among of the major multidrug efflux pumps [6–8], facilitating the expulsion of antibiotics, toxins and other materials from the bacterial cell. These RND efflux pumps, such as upregulated AdeABC and AdeIJK in *A. baumannii* (these are more crucial and commonly extrude chloramphenicol, tetracycline, fluoroquinolones, trimethoprim, as well as beta-lactams, macrolides, lincosamides, fusidic acid, novobiocin, and rifampicin), AcrAB-TolC in *E. coli*, EefAB-EefC in *K. pneumoniae*, and MexAB-OprM in *P. aeruginosa* (is capable of expelling

beta-lactams, macrolides, fluoroquinolones, and sulfonamides), have been extensively studied, revealing diverse roles in antibiotic resistance across these species. [9–12]

Therefore, there is a great demand for novel antibiotics or substrates to address Gram-negative strains that possess a second polar outer membrane and multiple efflux pumps, rendering them refractory to drugs.[13] But the discovery of novel antibiotics remains challenging due to underinvestment, low ROI, high attrition rates, and a lack of real innovation in the pipeline.[14] In this situation, Drug repurposing within next-generation combination approaches, known as antibiotic adjuvants, represents a promising strategy to combat MDR pathogens. This strategy helps sustain the therapeutic longevity of firmly established, clinically proven antibiotics.[15] One conspicuous success story for antibiotic-adjuvant combination therapy is the discovery of serine-β-lactamase inhibitors.[15–17] Hence, research efforts toward developing inhibitors of efflux pumps are a promising step, serving as antibiotic resistance breakers to resensitize inactive antibiotics against both innate and acquired MDR bacteria.[12, 18] The impacts of these inhibitors typically have two distinct outcomes: firstly, they restore the sensitivity of currently used antibiotics against MDR bacteria. Secondly, the ability to opt for resistant variants will diminish.[18]

To address this critical situation and restore the effectiveness of current antibiotics while preventing the emergence of new antibiotic resistance, our study has focused on combining antibiotics with non-antibiotics to target resistance mechanisms such as efflux pumps and biofilms. It aims to facilitate clinical translation of effective antimicrobial treatments by investigating synergistic adjuvant strategies. Therefore, we look for various non-antibiotics with varying degrees of broad-spectrum antibacterial activity, such as neuroleptics, antihistamines, antidepressants, antiplatelets, and nonsteroidal anti-inflammatory drugs (NSAIDs), through a literature review.[19] As demonstrated by the disk diffusion assay, we selected desloratadine and cetirizine (antihistamines), ambroxol (a mucolytic), and zinc gluconate (a zinc supplement) for further several studies.

Results

Disk Diffusion Assay

The antibacterial activity and the effect of obsolete antibiotics (ABs) and non-antibiotics (non-ABs) combinations against pathogenic bacteria are presented in **Table S1** (S indicates the supplementary file). Ambroxol, cetirizine, zinc gluconate, and desloratadine demonstrate antimicrobial effects against all tested pathogens when combined with the obsolete ABs. In most cases, the combination zone was enhanced; however, in some cases, the result was the opposite, resulting in a truncated combination zone. We can discuss these phenomena in terms of three effects: Synergism (weakly/slightly, moderately & highly), Antagonism, and No effect (Indifferent ZOI).[20]

In **Table S1**, we show that cetirizine and zinc gluconate exhibit no zone of inhibition against *P. aeruginosa* ATCC-27853, and that cetirizine alone shows no effect against *S. aureus* ATCC-25923. The combination approaches demonstrated a notable enhancement in the zone of inhibition against all microorganisms compared to the obsolete ABs alone. Our findings indicate that the combination of some obsolete ABs with non-ABs exhibited the antagonistic effect (such as levofloxacin + desloratadine against *E. coli* ATCC-25922: from 32 mm to 29 mm zones of inhibition, and chloramphenicol + cetirizine against *P. aeruginosa* ATCC-27853:

from 17 mm to 15 mm zones of inhibition), etc. On the other hand, some combinations displayed a promising & synergistic effect (such as oxytetracycline + desloratadine, erythromycin + desloratadine, against *A. baumannii* NCTC-12156: from 21 mm to 28 mm and 16 mm to 22 mm zones of inhibition, and oxytetracycline + zinc gluconate, erythromycin + zinc gluconate against *E. coli ATCC-25922*: from 21 mm to 29 mm and 16 mm to 20 mm zones of inhibition). Several in vitro studies have shown that zinc ions released from zinc salts suppress the growth of some bacterial strains, and desloratadine is also being investigated as a potential antibiotic combination to increase antibiotic efficacy and exhibit synergism against resistant bacterial strains. [21, 22] The main findings of this experiment are that when combined with ABs, these non-ABs medications exhibited potential synergistic effects. Evaluating the safety of these medications when combined with other ABs is essential. Overall, they are considered safe drugs with minimal and manageable side effects.

Minimum Inhibitory Concentration (MIC) Determination

The results of MIC of ABs, non-ABs, and their combinations are presented in Table 1 The non-ABs (such as ambroxol, cetirizine, zinc gluconate, and desloratadine) alone showed MIC values ranging from 64 to 512 µg/ml against the mentioned pathogens. In the case of *A. baumannii* NCTC-12156, the combinations resulted in a substantial fall in MIC relative to the individual antibiotic. In particular, MIC on positive control, erythromycin, was found at the sixth well (2–6 = 16 µg/ml) before the color shift occurred, where the values for the combination of erythromycin-desloratadine and erythromycin-zinc gluconate were observed at the tenth well (2–10), which was equivalent to 1 µg/ml. Furthermore, the values were 50% reduction from 16 µg/ml to 8 µg/ml for cetirizine and zinc gluconate, and also a two-fold reduction for desloratadine when combined with doxycycline rather than the control alone, decreasing from 16 µg/ml to 4 µg/ml. The azithromycin-ambroxol combination exhibited an antagonistic effect at concentrations, a range from 0.25 µg/ml to 0.5 µg/ml.

Additionally, the rest of combination did not demonstrate a notable reduction in MIC values against this pathogen. For *E. coli* ATCC-25922, none of the complexes of oxytetracycline, chloramphenicol, levofloxacin, or ciprofloxacin with non-ABs showed noticeable decreases in MIC values; in contrast, the doxycycline-zinc gluconate complex showed an antagonistic effect, increasing from 8 µg/ml to 16 µg/ml. Additionally, the erythromycin-desloratadine and erythromycin-zinc gluconate complexes showed a dramatic reduction in MIC values, five-fold & four-fold, respectively, from 32 µg/ml to 1 µg/ml and 2 µg/ml, respectively. Like that, these complexes also showed a 5-fold reduction in activity against *S. aureus* ATCC-25923, dropping from 16 µg/ml to 0.5 µg/ml. 50% values were reduced for the complexes of azithromycin-cetirizine and -desloratadine; on the other hand, a two-fold decrease (from 2 µg/ml to 0.5 µg/ml) was observed for azithromycin-zinc gluconate against *S. aureus* rather than the azithromycin alone.

Furthermore, the remaining combinations did not demonstrate any remarkable values against *S. aureus*. Afterward, significant changes in MIC values were observed for the drug combination against *P. aeruginosa* ATCC-27853, with a 3-fold reduction in the erythromycin-desloratadine combination, from 32 µg/ml to 4 µg/ml. In contrast, a 2-fold decline in erythromycin-zinc gluconate was observed, to 8 µg/ml compared to the control. In most cases, MIC values were the same as those for the control antibiotics. As for the overall outcome, we affirm that some promising combinations (such as erythromycin-desloratadine or erythromycin-zinc gluconate) can decline MIC values against resistant pathogens, thereby tackling antibiotic resistance. To further assess, *in vivo* experiments using a mouse model were also conducted in this study.

Table 1
represents the Minimum Inhibitory Concentration (MIC) values of obsolete ABs (Alone) and the combination of these ABs with non-ABs. Here, ABs indicate the antibiotics, and non-ABs means non-antibiotics.

Pathogens	Minimum Inhibitory Concentration (MIC)					
	Selected non-ABs		Ambroxol	Cetirizine	Zinc Gluconate	Desloratadine
	Selected ABs	Alone (ABs)	MIC(ug/ml)	MIC(ug/ml)	MIC (ug/ml)	MIC (ug/ml)
Acinetobacter Baumannii (NCTC-12156)	**Non-AB (Alone)**		128	256	128	64
	Oxytetracycline	4	4	4	4	4
	Chloramphenicol	64	64	64	64	64
	Doxycycline	16	16	8	8	4
	Azithromycin	0.25	0.5	0.25	0.25	0.25
	Erythromycin	16	4	32	1	1
	Moxifloxacin	0.25	0	0.25	0.5	0.25
	Gentamicin	0.5	0.5	0.5	0.5	0.5
	Levofloxacin	0.25	0.25	0.25	0.25	0.25
	Ciprofloxacin	0.5	0.5	0.5	0.5	0.5
Escherichia coli (ATCC-25922)	**Non-AB (Alone)**		256	256	128	128
	Oxytetracycline	4	4	4	4	4
	Chloramphenicol	64	64	64	64	64
	Doxycycline	8	8	8	16	4
	Azithromycin	1	1	0.5	0.25	0.5
	Erythromycin	32	16	64	2	1
	Moxifloxacin	1	0	0.25	0.25	0.25
	Gentamicin	1	0.5	0.5	0.5	0.5
	Levofloxacin	0.25	0.25	0.25	0.25	0.25
	Ciprofloxacin	0.5	0.5	0.5	0.5	0.5
Pseudomonas aeruginosa (ATCC-27853)	**Non-AB (Alone)**		64	256	128	128
	Oxytetracycline	4	4	4	4	4
	Chloramphenicol	32	16	16	16	32
	Doxycycline	8	8	8	16	4
	Azithromycin	1	1	0.5	0.5	0.5

	Erythromycin	32	16	32	8	4
	Moxifloxacin	2	2	1	1	1
	Gentamicin	0.25	0.25	0.25	0.25	0.25
	Levofloxacin	0.25	0.25	0.25	0.25	0.25
	Ciprofloxacin	0.5	0.5	0.5	0.5	0.5
Staphylococcus aureus (ATCC 25923)	**Non-AB (Alone)**		512	512	512	256
	Oxytetracycline	2	2	2	2	2
	Chloramphenicol	64	64	64	64	64
	Doxycycline	1	2	2	2	4
	Azithromycin	2	2	1	0.5	1
	Erythromycin	16	1	16	0.5	0.5
	Moxifloxacin	0.5	2	0.25	0.5	0.25
	Gentamicin	1	0.5	0.5	0.5	0.25
	Levofloxacin	0.25	0.25	0.25	0.25	0.25
	Ciprofloxacin	0.5	0.5	0.5	0.5	0.5

In vivo Experimental Outcomes

Observation of neutropenia and A. baumannii-induced lung infections

The result was as follows: the WBC count in the control group was 9.75 (thousand/mm3), and in the neutropenia group, it was 2.12 (thousand/mm3). The basal WBC count is a range of 80 to 85% below normal, indicating neutropenia.[23] In our experiment, around ~ 80% of WBC were reduced from the normal group. Sequentially, after inoculation of bacteria in mice by intranasally, for the observation of induction of lung infections, the inoculated bacterium was Gram-negative which was confirmed by the gram stanning process, shown at **Fig. 1**. Also, observed visible weight loss, lethargy, and appetite loss, and respiratory problems like faster heart rate, labored breathing, gasping, and wheezing due to the disease, which indirectly indicated the respiratory infections.

Body Weight Changes

The A. baumannii-induced lung infection mouse model was treated with a combination erythromycin-desloratadine and erythromycin-zinc gluconate, as well as erythromycin alone. The body weight of mice fluctuated during disease induction, with a drop observed in all groups except the control group, followed by steady recovery and weight gain, as shown in **Table S2** and Fig. 2**(a)**. According to the table, the control group showed gradual increases in body weight, as expected for a normal group. The diseased group showed a decrease in body weight after the onset of disease, such as erythromycin, erythromycin-zinc gluconate (Ery + ZnG), and erythromycin-desloratadine (Ery + Des) -treated groups, but slightly restored weight at day 4 and day

5; furthermore, there was a visible difference between the control and disease group at the day of onset. On the other hand, the erythromycin, Ery + ZnG, and Ery + Des-treated groups showed a significant decrease in body weight at day 2. But these groups restored their weight on another consecutive treatment day. Specifically, upon completion of treatment (Day 5), the erythromycin-treated group ($P < 0.05$, d = -1.46, power = 41%) did not show a significant restoration in body weight compared to the disease group. In contrast, the Ery + ZnG ($P < 0.05$, d = -2.77, power = 90%) and Ery + Des ($P < 0.01$, d = -4.8, power = 98%)-treated groups exhibited a greater recovery in the percentage change in body weight.

Total WBC count

The *A. baumannii*-induced lung infection in immunosuppressed mice results in a significant elevation of total white blood cell counts, both systemically in the bloodstream and locally in the lungs, which are indicative of an active immune response to eradicate the infection.[23] Regarding the WBC, Table 2 and Fig. 2**(b).** showed that the diseased group caused by *A. baumannii*-induced infection had a significantly increased WBC count, rising from 2.12 (thousand/mm³) before disease onset to 3.87 (thousand/mm³). This elevation of WBC count occurs as a direct immunological response to the infection. Furthermore, the WBC count in the control group remained relatively stable throughout the *in vivo* study, ranging from 9.25 (thousand/mm³) to 9.75 (thousand/mm³). In contrast, the Ery + Des -treated group ($P < 0.05$, d = 1.8, power = 57%) restored circulating WBC counts to near-normal levels after treatment, and no significant difference was observed. However, treatment with erythromycin alone (Ery group) moderately restored WBC counts compared with the disease group ($P < 0.01$, d = 3.16, power = 74%), consistent with its immune-regulatory effects, yet the difference was not statistically significant. In contrast, adjunct treatment groups {Ery + ZnG group ($P < 0.05$, d = 2.29, power = 77%) and Ery + Des group ($P < 0.01$, d = 3.98, power = 92%)} restored more circulating WBC counts than the Ery group, with a significant difference and augmented the host immune balance by attenuating the inflammatory stress.[24, 25]

Table 2
Contains the total WBC count and mean lung weight index (LWB) with SD of the different experimental groups when treated with an antibiotic and its combination. Here, FBW = Final Body Weight, LW = Lung Weight.

Group	**Total WBC count (thousand/mm^3) ± SD**	**FBW(mean) ± SD**	**LW(mean) ± SD**	**LWI(mean) ± SD**
Control Group	9.25 ± 0.81	36.54 ± 1.28	0.19 ± 0.016	0.52 ± 0.047%
Disease Group	3.87 ± 0.49	32.97 ± 0.60	0.25 ± 0.011	0.76 ± 0.036%
Ery Group	5.45 ± 0.51	32.81 ± 0.72	0.23 ± 0.010	0.70 ± 0.034%
Ery + ZnG Group	6.75 ± 0.62	33.49 ± 0.70	0.205 ± 0.011	0.61 ± 0.035%
Ery + Des Group	7.89 ± 0.70	32.95 ± 0.93	0.20 ± 0.015	0.60 ± 0.048%

Measurement of Lung Weight Index (dup: abstract ?)

Future research focused on creating efficient treatments for lung infection-related conditions can be guided by the steady rise in the lung weight index caused by *A. baumannii*, which emphasizes the inflammatory response.[26] In case of LWI, Table 2 and Fig. 2**(c)** showed that lung weight and index were significantly increased in *the A. baumannii*-induced diseased group compared with the control group, due to accumulation of inflammatory cells. In contrast, a significant weight declined in Ery + ZnG group ($P < 0.01$, $d = 4.22$, power = 95%) and Ery + Des group ($P < 0.01$, $d = 3.77$, power = 89%) than the disease group, where after treatment, Ery group alone showed no significant result than disease group ($P < 0.05$, $d = 1.71$, power = 53%). On the other hand, the Ery + Des group showed no significant difference from the control group ($P < 0.05$, $d = -1.68$, power = 52%), which indicated that the inflammatory response was decreased significantly in the Ery + Des group. Therefore, the combination strategies of Ery + Des ($P < 0.05$, $d = -2.40$, power = 81%) and Ery + ZnG ($P < 0.05$, $d = -2.61$, power = 86%) showed better curing capability and demonstrated a significant difference compared with erythromycin alone.

Histopathological analysis

In lung infection, the integrity of the alveolar walls can be significantly compromised, leading to various pathological changes, such as inflammatory response, alveolar wall thickening, diffuse alveolar damage (DAD), and exudation.[26] As the evident, the tissue sections of control mice as compared to that of the diseased group-showed the collapsed in alveolar, DAD, and considerable inflammatory cell infiltrations were shown at Fig. 3. However, the structure of tissue sections taken from Ery + Des and Ery + ZnG group mice compared with erythromycin (Ery) treated mice with was found almost normal; they had more integrity of alveolar cell, and less inflammatory reactions than standard group mice. However, the Ery + Des result shows that the tissue structure is better preserved than with Ery + ZnG, due to the anti-inflammatory effect of desloratadine (Des).[24] The results indicate that Ery + Des and Ery + ZnG can reduce pneumonia symptoms to a great extent in *A. baumannii*-induced pneumonia (ABIP).

In Silico Study

Predicted Resistance Genes via CARD resistance gene identifier (RGI)

The Comprehensive Antibiotic Resistance Database (CARD) RGI is a bioinformatics platform that predicts and annotates antibiotic resistance genes, their encoded products, and the associated resistance mechanisms. [27]. Using the Proksee tool on the CG View server, several classes of resistance genes (which contribute to major class of antibiotic resistance) in *A. baumannii* (NCTC-12156) were identified via CARD RGI, that are, as summarized at **Table S3** and illustrated shown in **Fig. 4**. From the all ORF_ID, we find out the only ORF_ID and resistance genes, which develop resistance on macrolide antibiotics class as erythromycin in this class. Among these, the *adeJ* gene exhibited the highest bitscore (2149.4) and approximately 100% identity, indicating a strongly conserved macrolide-resistant genotype. The *adeJ* gene encodes the AdeJ transporter protein, a major element of the AdeIJK efflux pump, indicated by a blue border circle in the figure. 4., which

belongs to the RND efflux transporters and plays a key role in AMR. AdeIJK pump expels substrates such as erythromycin, beta-lactams, fluoroquinolones, chloramphenicol, as well as tetracycline, trimethoprim, and rifampicin.[8, 10]

Molecular Docking Analysis

Protein-ligand docking is used to study the binding mechanism, binding sites, preferred orientations, complex stability, energy profiles, and bonding profiles.[28] The results of the molecular docking study targeting the efflux pump protein are presented in **Table S4 and** Fig. 5**(a–c)**, with desloratadine and zinc gluconate as the test ligands and erythromycin as the control. As shown in Table 8, the 7M4P + desloratadine complex and 7M4P + zinc gluconate complex displayed a binding affinity of − 9.9 kcal/mol and − 5.6 kcal/mol, respectively, whereas the control complex 7M4P + erythromycin exhibited − 10.1 kcal/mol. The ligands interacted with overlapping key residues of 7M4P, as shown in Fig. 5**(a), 5(b)**; desloratadine bound to Phe136, Val139, Ala326, Tyr327, Phe611, Phe629 with nine (09) hydrophobic interactions {Pi-Alkyl (05), Pi-Pi T-shaped (01), Pi-Pi Stacked (01) and Alkyl (02)} improve mechanical robustness and long-term integrity by resisting dissociation of complex, play the vital role for persistent inhibitor binding in efflux pumps.[29] Then, zinc gluconate formed five hydrogen bonds with Tyr35, Ser135, Phe136, and Thr329. A higher hydrogen bond number also demonstrates enhanced complex stability and integrity, indicating a major inhibition of efflux pumps.[30] In contrast, erythromycin, as a control, interacted with Ser79, Asn81, Gln91, Phe618, Glu675, and Gln685 with three hydrogen bonds, two Pi-Alkyl bonds, one unfavorable donor (4.11 Å), and one unfavorable acceptor (4.95 Å).

Root Mean Square Deviation (RMSD) analysis

To evaluate conformational change and structural stability of the protein–ligand complexes, MD simulations lasting 100 ns were conducted for the three compounds (desloratadine, CID 124087; zinc gluconate, CID 443445; and erythromycin, serving as a control, CID 12560) with the protein (PDB ID: 7M4P) and the apo-protein, analyzing the result plotted by root mean square deviation (RMSD) values versus time in Fig. 6**(a)**. During the analysis, the protein complex of desloratadine and the control displayed almost the same stable equilibrium with minor trajectories, yet desloratadine presented the most stable interaction with the protein throughout the range of 30–35 ns and 60–73 ns, with 2.8 Å and 5.0 Å, respectively. In contrast, moderate fluctuations were shown in the zinc gluconate complex and apo-protein, indicating moderate structural stability compared to the others.

Root Mean Square Fluctuation (RMSF) analysis

Root Mean Square Fluctuation (RMSF) for each residue of protein in its apo form and complexed with desloratadine, zinc gluconate, and erythromycin (control) was carried out using a 100 ns MD simulation for analysis, as shown in Fig. 6**(b).** The data results showed that desloratadine had significantly lower RMSF, which means it involves less residual flexibility (more structural stability) than erythromycin from an overall scan of 1000 residues. Conversely, RMSF values were relatively high for zinc gluconate and the apo form of the protein, indicating flexibility and decreased stability. In conclusion, according to RMSF analysis, desloratadine had a stabilizing effect on the protein structure much greater than either the control or zinc gluconate.

Solvent Accessible Surface Area (SASA) analysis

The solvent-accessible surface area (SASA) of proteins has consistently been regarded as a critical factor in the study of protein folding and stability.[31] Residues with low SASA values are more densely packed and have less solvent exposure, whereas residues with high SASA values are the opposite.[32] This graph, as shown in Fig. 6**(c)**, demonstrates the SASA of four systems over 100 ns. Every system's SASA values evolve, indicating that their exposure to the solvent changes over time. Since erythromycin has the most observed changes, it likely had the most exposure on its surface throughout the analysis. In contrast, zinc gluconate had more stable SASA profiles: it started at 470 nm² and, over the 16–58 ns range, exhibited the lowest values, 446–448 nm², respectively, indicating less solvent exposure and greater stability with the protein. Also, desloratadine showed more stable densities than erythromycin (control) throughout the analysis, especially in the ranges 52 ns to 74 ns and 92 ns; it provided the lowest values of 460 nm² to 462 nm² and 460 nm², respectively. The Apo state was initially presented as slightly solvent accessible and changed less than other states after 30 ns.

Radius of Gyration (Rg) analysis

In a 100 ns simulation, the apo form of the protein initially displayed lower Rg values but increased conformational flexibility after 5 ns. Conversely, the control, erythromycin (CID 12560)-7M4P complex exhibited relatively higher Rg values throughout the simulation, accompanied by more noticeable fluctuations from 3.63 nm to 3.80 nm, indicating a less compact and comparatively more dynamic structural flexibility, as shown in Fig. 6**(d)**. Whereas desloratadine (CID 124087) initially showed fluctuations; but, after 43 ns of analysis, it sustained lower Rg profiles (from 3.58 nm to 3.70 nm) throughout the majority of the trajectories, and also zinc gluconate (CID 443445) maintained 3.60 nm to 3.70 nm Rg values after 7 ns of dynamics, suggesting both have greater compactness and improved conformational stability with protein 7M4P.

Interpretation of Principal Component Analysis (PCA)

To achieve a deep knowledge of protein domain motion patterns along with the extent of conformational changes upon ligand binding, PCA analysis was done for the desloratadine (CID 124087)-7M4P complex, the zinc gluconate (CID 443445)-7M4P complex, the control, erythromycin (CID 12560)-7M4P complex, and the apo protein. In our study, the chromatic graphs generated from various protein configurations are plotted as dots, each representing a unique configuration. During the simulation, the color of the dots shifts in a time-dependent manner from blue to green to yellow, indicating conformational changes within the protein. In Fig. 7**(a-d)**, blue portrays the first timestep, while green and yellow represent the middle and last timesteps, respectively. PCA revealed three principal components (PCs) through molecular dynamics trajectories, elucidating the motion of a notable segment of the protein structure. From Fig. 7**(a-d)**, the apo-protein (7M4P), desloratadine (CID 124087), zinc gluconate (CID 443445), and erythromycin (CID 12560) in the system contributed to 66%, 49.5%, 77.5%, and 67% of the variations, respectively. A higher contribution in variations indicates a destabilization trend, and a lower contribution indicates a stable complex and collective movement in a biological system.[32] The PC1 value of the control, erythromycin (CID 12560)-7M4P complex was 67%, and the lowest, except for the PC1 value of apo 7M4P.

Free energy landscape (FEL) analysis

To better understand the conformational change in a comprehensive system, the free energy landscape (FEL) was investigated.[33] To comprehend the minimal free energy of the Cα backbone atoms regarding stability,

FEL was computed for desloratadine (CID 124087)-7M4P complex, zinc gluconate (CID 443445)-7M4P complex, erythromycin (CID 12560)-7M4P complex, and apo-7M4P. The first two primary components of the complexes, PC1 and PC2, were plotted to make an FEL graph. The change from violet to red in Fig. 7**(a-d)** indicates a change in Gibbs free energy. Red denotes a high-energy, unstable system, while violet denotes a low-energy, more stable system. A complex loses energy during stabilization, and its energy state turns red instead of violet. A single energy basin with stable free energy minima indicates a stable structure.[34] On the other hand, several energy basins reflect more conformational variation and the formation of a loop-like shape. For the desloratadine (CID 124087)-7M4P complex, we found persistent free-energy minima within a single energy basin. The three other complexes had several expansive and metastable energy basins, indicating that their conformations changed throughout the 100 ns simulation, and finally, all of the complexes became progressively stable.

Binding free energy analysis

We used the molecular mechanics/Poisson–Boltzmann surface area (MM/PBSA) method to measure the binding free energies of three complexes. This method renders it easier to break down the total binding energy (ΔG) into its components, leading to it possible to examine closely at how the interactions between the ligand and the target protein affect the energy, as shown in Table 3 **and Figure S1**. Notably, both the desloratadine (CID 124087) and zinc gluconate (CID 443445) complexes suggested the most favorable binding affinity by ΔG of -20.37 ± 0.51 and − 18.37 ± 0.46 kcal/mol respectively than the control, erythromycin (-12.37 ± 0.51) kcal/mol. Although the net solvation energy (ΔGSOLV = 41.65 ± 0.66 kcal/mol) partially opposed binding, the strong gas-phase interactions (-61.83 ± 1.10 kcal/mol), electrostatic energy (-21.15 ± 0.85 kcal/mol), ΔVDWAALS (-40.68 ± 0.46 kcal/mol), and ΔG ensured overall structural stability of desloratadine (CID 124087) complex. Afterward, zinc gluconate (CID 443445) complex exhibited better ΔVDWAALS, ΔESURF, and ΔGSOLV values than the control. Additionally, the small standard deviations in zinc gluconate (CID 443445) complex suggested the high level of reliability and reproducibility in the binding energy estimations.[33]

Table 3
Analysis of MM/PBSA of three complexes with 7M4P (a) desloratadine (CID 124087), (b) zinc gluconate (CID 443445) and (c) control, erythromycin (CID 12560.

Energy components/complexes	**Desloratadine (CID 124087)**	**Zinc gluconate (CID 443445)**	**Erythromycin (CID 12560) [Control]**
Van der Waal energy (ΔVDWAALS)	-40.68 ± 0.46	-31.41 ± 0.38	-19.07 ± 0.25
Electrostatic energy(ΔEEL)	-21.15 ± 0.85	-2.80 ± 0.47	-17.27 ± 0.71
Polar solvation energy (ΔEGB)	47.52 ± 0.70	19.69 ± 0.33	27.51 ± 0.47
Non-polar solvation energy (ΔESURF)	-5.87 ± 0.08	-3.85 ± 0.04	-3.54 ± 0.03
Net gas phase energy (ΔGGAS)	-61.83 ± 1.10	-34.21 ± 0.69	-36.34 ± 0.71
Net solvation energy (ΔGSOLV)	41.65 ± 0.66	15.84 ± 0.32	23.97 ± 0.48
ΔG (total binding free energy)	**-20.18 ± 0.67**	**-18.37 ± 0.46**	**-12.37 ± 0.51**

Discussion

Several mechanisms, such as upregulation of efflux pumps and biofilm development, synergistically drive the emergence of antibiotic resistance, serious health issues globally, and the failure of conventional therapies, thereby sustaining persistent infections. A recent study by Silvia Vareschi et al. examined the interconnection between efflux pumps and biofilm formation through a self-reinforcing cycle that promotes bacterial persistence. Efflux pumps aid in biofilm development by exporting quorum-sensing molecules and iron-scavenging siderophores, while biofilm growth increases efflux pump expression, thereby enhancing antibiotic resistance. The AcrAB-TolC efflux pump in *E. coli*, for which the AcrB and TolC components have been found to play a structural role in cell envelope stability, is a key contributor in forming biofilm.[35] In the presence of azithromycin, the MexAB-oprM and MexCD-oprJ efflux systems were crucial for biofilm development, and the MexCD-OprJ efflux system was upregulated in *P. aeruginosa* biofilms. Evidence suggests that during biofilm development, *S. aureus* showed increased relative expression of the genes encoding the MFS, NorB, and NorC efflux pumps. [36]

This bidirectional interplay elucidates the endurance of biofilm-associated conditions and emphasizes the efflux pump inhibitors (EPIs) as potential candidates to eradicate biofilms and rejuvenate antibacterial effectiveness.[37] Research on clinical isolates of *K. pneumoniae* found that reserpine, an EPI, inhibited biofilm formation at 15.83 mg/L. In contrast, 2mg/L of CCCP and 16mg/L PABN were investigated by Baugh et.al. to disrupt the *S. aureus* biofilms 5-fold and *E. coli* biofilms formation, respectively. Also, high concentrations of EPIs are needed to inhibit *P. aeruginosa* biofilms.[36, 38] Therefore, finding the potential candidate as an efflux pump inhibitor may be expensive and time-consuming. But it is rational to investigate certain drugs with known pharmacokinetics and toxicokinetics that currently employe in clinical practice as potential inhibitors. Although drug selection may pose challenges, it may be easier to select the drugs that have proven synergistic antibacterial effects when combined with antibiotics, such as macrolides, tetracyclines, fluoroquinolones, or quaternary amine-containing antiseptic agents, because these antibiotics recognize as efflux pump substrates.[39]

Our study has rigorously investigated desloratadine and zinc gluconate as adjuvants that synergize with antibiotics to combat MDR bacteria by inhibiting efflux pump overregulation and biofilm formation. Desloratadine is a 2nd gen., non-sedating, long-acting tricyclic antihistamine drug. Nikoletta Szemerédi et al. reported that antihistamines such as promethazine, significantly inhibited the activity of efflux pump in all tested *E. coli* strains, with 50% of strains showing reduced biofilm formation.[40] Another in vitro and *in vivo* finding reported that the combination of desloratadine with meropenem reduced the MIC by twofold and increased antibiofilm activity by eightfold, providing significant protection of up to 83% of Caenorhabditis elegans infected with MDR *A. baumannii*.[22] In contrast, zinc gluconate is a zinc salt of gluconic acid, often taken as a zinc supplement and also demonstrated inhibitory activity against opportunistic pathogens, as well as implicated in several infections.[41] A previously in vitro and *in vivo* report by Brigitte D. et al. found that the addition of zinc salts reduced the resistance of *Propionibacterium acnes* strains to erythromycin.[42] The 2024 study by Mohammad H. S. et al. suggested that co-administration of ciprofloxacin and zinc oxide nanoparticles may reduce the overexpression of the NorA and NorB efflux pumps in *S. aureus*, thereby preventing the overabundance of pumps and the emergence of resistance.[43]

Building on these findings, our study demonstrated different combinations of desloratadine, and zinc gluconate with conventional antibiotics against specific pathogens, thereby extending the scope beyond previous studies, where desloratadine, and zinc gluconate markedly enhances the antimicrobial activity of erythromycin, as evidenced by a decline of MIC, shown at Table 1, in vitro, alongside a mouse lung infection model also confirmed the biological significance of the Ery + Des and Ery + ZnG combination against *A. baumannii* NCTC-12156. The results demonstrated that Ery + Des and Ery + ZnG combination were significantly more effective than erythromycin alone to restore the body weight ($P < 0.01$, $d = -4.8$, power = 98%) and ($P < 0.05$, $d = -2.77$, power = 90%), to recover WBC counts ($P < 0.01$, $d = 3.98$, power = 92%) and ($P < 0.05$, $d = 2.29$, power = 77%), and to inflammatory response decrease ($P < 0.05$, $d = -2.40$, power = 81%) and ($P < 0.05$, $d = -2.61$, power = 86%), respectively. In addition to lung histopathology, more intact alveolar cells and less inflammation were observed in Ery + Des than in Ery + ZnG, due to desloratadine's anti-inflammatory effects. [24] Complementing these biological findings, in silico analyses revealed the binding sites, preferred orientations, and energy profiles of desloratadine, zinc gluconate, and erythromycin with the efflux protein AbeJ (7M4P). During MM/PBSA analyses, desloratadine (CID 124087) and zinc gluconate (CID 443445) complexes appeared as the most promising compounds, occupying their key residues and exhibiting more negative binding free energies of -20.37 ± 0.51 and − 18.37 ± 0.46 kcal/mol, respectively, than the control, erythromycin. PCA analyses revealed that the 7M4P + desloratadine complex contributed less to variation, indicating well-defined, conformationally stable states in a biological system over a 100 ns MD simulation.[32] Furthermore, analyses of RMSD, Rg, SASA, and FEL indicated that the desloratadine (CID 124087)-7M4P and zinc gluconate (CID 443445)-7M4P complexes maintained high to moderate stability throughout the period.

Collectively, these results suggest that desloratadine and zinc gluconate are promising candidates for EPIs by disrupting biofilm integrity and efflux pumps [22][43], thereby restoring the potency of erythromycin through synergistic activity. In contrast to previous studies focused on either efflux pumps or biofilms, our results demonstrate the enhanced activity achievable through simultaneous targeting of multiple resistance mechanisms. This strategy may reduce required doses and combat MDR strains. Although constrained by drawbacks of animal models and the need for biochemical substantiation of in silico predictions, these results serve to prioritize future translational research on adjuvant strategies, the mechanistic view of the efflux–biofilm interconnection, and clinically relevant infections.

Conclusion

The alarming rise in antibiotic resistance is evident, as MDR bacteria are emerging that can resist even last-resort treatments. The strict requirements and growing resistance are impeding the finding of novel antibiotics. At this time, investigating the mechanisms of resistance to current antibiotics and addressing ways to improve their effectiveness through non-antibiotic agents, termed antibiotic adjuvants, is advisable. Our studies reveal that the non-antibiotic compounds, desloratadine and zinc gluconate, may serve as promising antibiotic adjuvants that restore erythromycin efficacy, as shown in the studies above. A significant synergistic effect with erythromycin was observed in vitro, including ZOI enlargement and decreased MICs. These results are substantiated by an animal model, where adjuvant therapy boosted clinical efficacy, demonstrating bench-to-bedside relevance. In silico analyses, such as MD simulations, also demonstrated the stable interactions of these compounds with the efflux pump protein AdeJ, leading to inhibition of efflux activity linked to biofilm formation and resistance in *A. baumannii*. Therefore, both preclinical and

computational data suggest that the combination of erythromycin-desloratadine and erythromycin-zine gluconate may be potential candidates to rejuvenate erythromycin efficacy as adjuvant therapy; however, before translation into clinical use, it is necessary to conduct further clinical research and validate their ability to inhibit efflux pumps in other species.

Methods And Materials

All chemicals and analytical reagents were purchased from Sigma Chemical Co. (St. Louis, MO, USA). The mentioned drugs requisitioned from several pharmaceutical companies: ciprofloxacin, azithromycin, levofloxacin, erythromycin, doxycycline (Square Pharmaceuticals PLC, Bangladesh); gentamicin, chloramphenicol, desloratadine, ambroxol, zinc gluconate, and cetirizine (Incepta Pharmaceuticals Ltd., Bangladesh).

Bacterial isolates

Five bacterial strains used in the bacterial susceptibility assay. One strain used for the *in vivo* study: Multidrug Resistant (MDR) *Escherichia coli* (ATCC-25922), *A. baumannii* (NCTC-12156), *Pseudomonas aeruginosa* (ATCC-27853), *Shigella boydii* (CRL), Methicillin Resistant *Staphylococcus aureus* (MRSA)- ATCC 25923, and *Bacillus cereus* (ATCC-11778). Bacterial strains derived from the Culture Collection Unit, Department of Microbiology, ICDDRB, Dhaka, Bangladesh.

Bacterial Susceptibility Assay

Disk Diffusion Assay

The EUCAST disk diffusion assay is a proven, widely used method for antimicrobial susceptibility testing, employed in standard clinical laboratory settings.[44] For assessing the synergism of antibiotics (ABs) and non-antibiotics (non-ABs), each bacterial suspension (0.5 McFarland standard; 1–2 × 108 CFU/mL) spread onto sterile Muller-Hinton (MH) agar plates with the aid of a pre-sterilized cotton swab. Afterward, pre-sterilized Whatman filter paper disks (around 6 mm in diameter with 20µl dispensed volume) were infused with the different ABs (20µg/10µl/disk) or the non-ABs (20µg/10µl/disk), or the combination of AB and non-AB (20µg/ 10µl and 20µg/ 10µl /disk), and placed on the previously swabbed bacterial agar plates, that let to spread at 4°C in a refrigerator for 30–45 minutes and then inoculated overnight at 37°C. To conclude, the zone of inhibition (ZOI) was determined.[45]

Resazurin-based Turbidometric test and MIC assessment

Preparation of bacterial suspension

Three to four distinct colonies of sub cultured bacteria with identical morphologies were shifted into 10ml of sterile saline. According to the CSLI guidelines, the bacterial suspension was prepared with OD600 value calibrated, and then adjusted to 5 × 10^5 CFU/mL via a serial dilution. [46]

Preparation of the 96-well plates

MIC determinations of different ABs combined with non-ABs on bacteria were performed using the broth microdilution method according to standard microbiology and pharmacology procedures. The attained concentrations of the different ABs and their combinations were as outlined: 1024 to 1 µg/ml and 512 to 0.5 µg/ml for erythromycin and ciprofloxacin, respectively, with their combination, poured into 96 plates. Afterward, 50 µL of bacterial suspension (5×10^5 CFU/mL) was inoculated overnight at 37°C, then 50 µL of previously prepared resazurin solution (0.0075 mg/mL) was added, and the plates were again incubated for 2–4 hours at the same temperature. Finally, the color change of the wells was examined, and the lowest concentration was evaluated based on the MIC value.[46]

Animal Studies

After 7 days of adaptation to the surrounding environment, the mice were assigned to 5 groups (4 mice/group) for the investigation, as shown in **Table S5.**

Induction of neutropenia

Cyclophosphamide Monohydrate ('Cycloph', a branded product of Eskayef Pharmaceutical Ltd) was prepared to a final concentration of 1% by dissolving it in distilled water for injection. A total dose of 250 mg/kg was administered in two intraperitoneal injections to each mouse on days − 4 (150 mg/kg single dose) and − 1 (100 mg/kg single dose). To confirm neutropenia induction, mice were sacrificed and counted, and the WBC count in cyclophosphamide-injected mice was compared with that of normal mice. Afterward, mice were randomized to treatment and infection groups.[47]

Bacterial Inoculum preparation for lung infection

Mice were infected with *A. baumannii* NCTC-12156, which was grown overnight on MacConkey agar at 37°C. On the day of infection, a few colonies were suspended in 5 mL of sterile Luria-Bertani (LB) broth (Sigma-Aldrich, Italy). Following that, the turbidity of the bacterial suspension was adjusted to comply with the 0.5 McFarland standard, or roughly 1–2×10^8 CFU/ml. The bacterial suspensions were diluted at the right time to get the necessary concentration to cause the lung infection, approximately 6 Log_{10} CFU/ml to 8 log_{10} CFU/ml of *A. baumannii* NCTC-12156.[47, 48]

Intranasal inoculation infection

Mice (n = 20) were inoculated with bacterial suspensions (50µL) of *A. baumannii* NCTC-12156 by the aid of a micropipette. The release rate was properly maintained to ensure the mouse inhaled the inoculum without forming bubbles. To ensure persistent inoculation, mice were maintained in an upright position during the procedure and allowed several additional minutes for their breathing to stabilize.[47]

Confirmation of bacterial infections

After intranasal inoculation of bacteria into mice to confirm *A. baumannii*-induced lung infection, two mice were randomly selected from the diseased group, then sacrificed, and finally, blood was collected. After that, the blood culture was performed on nutrient agar, and the targeted bacteria were isolated based on their appearance. Also, the Gram staining procedure was performed on this bacterium. Finally, the visible and external signs in the mice were observed.[49]

Body Weight Assessment

A four-digit weight scale was used to measure weight on the 1st day of the disease induction and subsequently on the 2nd, 3rd, 4th, and 5th days of the treatment period.

Biological sample analysis

For biological sample analysis, mice were euthanized in the present study following approved ethical guidelines using a two-stage procedure. Isoflurane (4%) was first administered by the drop method in a tightly sealed induction chamber until the animals became fully unconscious. After confirmation of deep anesthesia, cervical dislocation was performed to complete euthanasia, followed by collecting the biological samples.[30]

White blood cell count (WBC)

This analysis was conducted by the blood samples were collected in EDTA tubes. Using the aforementioned technique, an automated veterinary hematology counter, POC H-100iV Diff™ (Sysmex®-Roche), was used to perform WBC counts.

Measurement of Lung Weight Index

In infectious models, lung weight index (LWI) measurements are essential for determining the effectiveness of treatment measures and comprehending the mechanisms underlying the disease. That's why, after the dissection of mice, the group-wise mice's lungs were carefully excised and washed with sterile saline. The lung weight was measured, following the calculated lung weight index (LWI) using the equation (lung weight/body weight) x 100 [50], and the lungs were finally stored group-wise in 10% Neutral buffered formalin solution for further analysis.

Histopathological Analysis

To investigate the prophylactic effects of the treatment groups against *A. baumannii*-induced lung infection, the lungs of sacrificed mice were weighed, and photographs were taken to assess inflammation. A segment of the lung was preserved in 10% (v/v) buffered formaldehyde and maintained at ambient temperature for sectioning. The lung slices (5 µm) were subjected to hematoxylin and eosin (H&E) staining and subsequently analyzed by transmission electron microscopy. Histological damage was assessed by evaluating the severity of lung tissue injury and neutrophil infiltration.[48]

Ethical Statement

The authors affirm that all procedures were carried out in accordance with relevant regulations and standards. The authors followed the "Animal Research: Reporting of In vivo Experiments" (ARRIVE) guidelines. The study was carried out in compliance with the ethical standards and regulations, as authorized by the Institutional Animal, Medical Ethics, and Biosecurity Committee (IAMEBBC) for Experimentations on Animal, Human, Microbes and Living Natural Sources of the Institute of Biological Sciences, University of Rajshahi, Bangladesh, as reported in the 36th meeting held on 26 May, 2025. (Memo No:151/320(48)/IAMEBBC/IBSc).

In Silico Study

Data Acquisition and prediction of resistance gene using CARD within a whole genome sequence

Bacterial genomes are widely utilized by virtually to comprehend evolutionary associations and the genetic basis of biological features such as virulence, antibiotic resistance, and metabolic capabilities.**[51]** To predict resistance genes from the whole-genome sequence of *A. baumannii* NCTC-12156, sequences (Accession no. GCA_900444725) were retrieved from the European Nucleotide Archive (ENA) in FASTA format. Subsequently, the FASTA-formatted sequences were uploaded to the Proksee tool on the CG View server (https://cgview.ca/), where a WGS base-pair map was generated based on GC content and GC skew. Furthermore, when the CARD resistance gene identifier (RGI) tools were used, the predicted resistance genes of *A. baumannii* NCTC-12156 were displayed in the WGS map. From the prediction results, key fields of these resistance genes were extracted into a CSV file: ORF_ID, Contig, Start, Stop, Orientation, Best Hit ARO/ARO ID, Best Identities (%), Drug Class, Resistance Mechanism, and AMR Gene.

Ligand & Protein Preparation

3D structures of three ligands were downloaded from PubChem [Desloratadine (CID: 124087) and Zinc gluconate (CID: 443445)] in ‘SDF’ format, and ChemSpider (Erythromycin; ID: 12041) in ‘MOL’ format. After that, the 3D structure of the predicted resistance gene-encoded protein {AdeJ; PDB ID: 7M4P (Chain-B)}, part of the AdeIJK efflux pump on the RND pump system in *A. baumannii* that expels antibiotics such as erythromycin, fluoroquinolone antibiotics, β-lactam antibiotics from inside the bacterial cell, and makes a major contribution to AMR, **[10]** was retrieved from www.rcsb.org in PDB format. Following that, the protein file was opened and prepared in Discovery Studio Visualizer v25.1.0.24284 to remove the natural ligand still attached, heteroatoms, and other unwanted elements. Afterward, the protein sequence was energy-minimized in Swiss-PDB Viewer v4.1.0 using the GROMOS96 force field.**[52]**

Molecular Docking Study

PyRx software v0.8 https://sourceforge.net/projects/pyrx/ with the AUTODOCK Wizard program was used to perform site-specific molecular docking of the following ligands with predicted resistance gene-encoded protein [AdeJ; PDB ID: 7M4P (Chain-B)}**[10]**. Firstly, the protein structure is loaded and subsequently made into a macromolecule. Afterward, the ligands were loaded into the control panel from OpenBabel, and energy minimization using the MMFF94 (Merck Molecular Force Field) steepest descent algorithm was performed; the resulting structures were subsequently converted to PDBQT format. Secondly, the amino acids F136, V139, F178, G179, F277, A326, Y327, F611, V613, F616, F629, F618, M666, L668, P671 to A680, R701, R718, T831 of the among proximal, F-loop and distal pocket**[8]**, was specified and set the grid box size and the centre of the docked complexes, respectively: box size: X=33.1282 Å, Y=36.4621 Å, Z=34.6064 Å; centre: X=208.3013 Å, Y=62.6241 Å, Z=215.7175 Å. Targeted docking method was used in this research, with the coordinate of origin set at X: 34.1808 Å, Y: 36.5314 Å, and Z: 33.2296 Å. Finally, the pose with the lowest RMSD and binding energy for each complex was selected for subsequent analysis.

Molecular dynamics (MD) simulation

MD simulation is a major approach for providing insights into conformational modifications, clarifying the dynamic stability of protein–ligand interactions over a predetermined time frame in a controlled environment. **[32,33]**. To deepen the understanding of binding interactions and molecular characteristics of three ligands with a target protein, we performed a 100-ns MD simulation with GROMACS (v2025.2), using the CHARMM36-JUL2022 force field.**[53]** The water model, TIP3P was used as the solvation method within a cubic simulation cell under physiological conditions, including a temperature of 300 K and pH 7.4, with 0.9% Na+ and Cl+ ions. **[54]** Initial energy minimization was achieved using simulated annealing with steepest descent. Long-range electrostatic interactions were accurately calculated and plotted in Python, with a timestep of 2 fs. The trajectory data were recorded every 0.002 ps, and simulations were run for 100 ns under 1 bar pressure, maintained by the Berendsen barostat. **[55]** Further analyses that included binding free energies (MM/PBSA), PCA, FEL, RMSD, Rg, RMSF, and SASA demonstrated a comprehensive understanding about the dynamic system.**[32]**

Statistical analysis

GraphPad Prism (v8.0.2) was used for statistical analysis. Tukey's multiple-comparison test was used to calculate P-values for the one-way ANOVA. The mice's lung weight, total WBC count, and percentage change in body weight were measured. Statistical power analysis was performed using RStudio software (v2025.09.2 Build 418), where achieved power was computed based on effect size (Cohen's d), sample size, and significance level (α). **[56]**

Declarations

Data availability statement

All relevant data in the study are included in the article and its supplementary information. Additional data are available from the corresponding author upon reasonable request

Author Contributions

R. M.: wrote the original draft, conducted all experiments, curated the data, performed data analysis, and data interpretation. **C. B.:** software, and performed data analysis **R. H. R.:** provided resources and conceptualization. **A. H.:** provided resources. **M. A. A. A.-B. :** conceptualization and supervision; reviewed and edited the original draft.

Competing interests

The authors declare no competing interests.

Funding

The corresponding author declares that no funds or grants were received for conducting this study.

Acknowledgement

The authors gratefully acknowledge Square Pharmaceuticals PLC and Incepta Pharmaceuticals Ltd. for providing some raw material of drugs required for this study.

Additional information

Correspondence and requests for materials should be addressed to M.A.A.A.-B.

References

1. Ho, C. S. et al. Jan. Antimicrobial resistance: a concise update. In: The Lancet Microbe, vol. 6, no. 1. Preprint, Elsevier Ltd, 1 https://doi.org/10.1016/j.lanmic.2024.07.010. (2025).
2. Liu, Z. et al. Drug Repurposing: Research Progress of Niclosamide and Its Derivatives on Antibacterial Activity. In: Infection and Drug Resistance. Preprint, Dove Medical Press Ltd, 17.4539–4556. https://doi.org/10.2147/IDR.S490998. (2024).
3. Naghavi, M. et al. Global burden of bacterial antimicrobial resistance 1990–2021: a systematic analysis with forecasts to 2050. *Lancet* **404** (10459), 1199–1226. https://doi.org/10.1016/S0140-6736(24)01867-1 (2024).
4. World Health Organization. Global Antibiotic Resistance Surveillance Report 2025 WHO Global Antimicrobial Resistance and Use Surveillance System (GLASS). Geneva. (2025). https://www.who.int/publications/i/item/9789240116337 (12 Apr. 2026, date last accessed).
5. Brown, D. Dec. Antibiotic resistance breakers: Can repurposed drugs fill the antibiotic discovery void? In: *Nature Reviews Drug Discovery*, no. 12. Preprint, Nature Publishing Group, 1 14.821–32. (2015). https://doi.org/10.1038/nrd4675
6. Gordon, N. C. & Wareham, D. W. Mar. Multidrug-resistant Acinetobacter baumannii: mechanisms of virulence and resistance. In: International Journal of Antimicrobial Agents, no. 3. Preprint, 35.219–226. https://doi.org/10.1016/j.ijantimicag.2009.10.024. (2010).

7. Klenotic, P. A. et al. Structural and Functional Diversity of Resistance-Nodulation-Cell Division Transporters. In: *Chemical Reviews*, 9. Preprint. *Am. Chem. Soc.* **12**, 121.5378–5416. https://doi.org/10.1021/acs.chemrev.0c00621 (May 2021).
8. Zhang, Z. et al. Cryo-em determination of eravacycline-bound structures of the ribosome and the multidrug efflux pump adej of acinetobacter baumannii. *MBio* **12** (3). https://doi.org/10.1128/mBio.01031-21 (2021).
9. Dulanto Chiang, A. & Dekker, J. P. Efflux pump-mediated resistance to new beta lactam antibiotics in multidrug-resistant gram-negative bacteria. *Commun. Med.* **4** (1). https://doi.org/10.1038/s43856-024-00591-y (2024).
10. Darby, E. M. et al. RND pumps across the genus Acinetobacter: AdeIJK is the universal efflux pump. *Microb. Genom*. **9** (3). https://doi.org/10.1099/mgen.0.000964 (2023).
11. Ornik-Cha, A. et al. Structural and functional analysis of the promiscuous AcrB and AdeB efflux pumps suggests different drug binding mechanisms. *Nat. Commun.* **12** (1). https://doi.org/10.1038/s41467-021-27146-2 (2021).
12. Duffey, M. et al. da May. Extending the Potency and Lifespan of Antibiotics: Inhibitors of Gram-Negative Bacterial Efflux Pumps. In: *ACS Infectious Diseases*, no. 5. Preprint, American Chemical Society, 10 10.1458–82. (2024). https://doi.org/10.1021/acsinfecdis.4c00091
13. Myers, A. G. & Clark, R. B. Discovery of Macrolide Antibiotics Effective against Multi-Drug Resistant Gram-Negative Pathogens. *Acc. Chem. Res.* **54** (7), 1635–1645. https://doi.org/10.1021/acs.accounts.1c00020 (2021).
14. Miethke, M. et al. Oct. Towards the sustainable discovery and development of new antibiotics. In: *Nature Reviews Chemistry*, no. 10. Preprint, Nature Research, 1 5.726–49. (2021). https://doi.org/10.1038/s41570-021-00313-1
15. Liu, Y. et al. Drug repurposing for next-generation combination therapies against multidrug-resistant bacteria. In: *Theranostics*, 10. Preprint. *Ivyspring Int. Publisher*. **11**, 4910–4928. https://doi.org/10.7150/thno.56205 (Mar. 2021). 4.
16. Dhanda, G., Acharya, Y. & Haldar, J. Mar. Antibiotic Adjuvants: A Versatile Approach to Combat Antibiotic Resistance. In: *ACS Omega*, no. 12. Preprint, American Chemical Society, 28 8.10757–83. (2023). https://doi.org/10.1021/acsomega.3c00312
17. Brem, J. et al. Structural basis of metallo-β-lactamase, serine-β-lactamase and penicillin-binding protein inhibition by cyclic boronates. *Nat. Commun.* 7. https://doi.org/10.1038/ncomms12406 (2016).
18. Zhang, L. et al. Feb. Bacterial Efflux Pump Inhibitors Reduce Antibiotic Resistance. In: *Pharmaceutics*, vol. 16, no. 2. Preprint, Multidisciplinary Digital Publishing Institute (MDPI), 1 (2024). https://doi.org/10.3390/pharmaceutics16020170
19. Lagadinou, M. et al. Mar. Antimicrobial properties on non-antibiotic drugs in the era of increased bacterial resistance. In: *Antibiotics*, vol. 9, no. 3. Preprint, MDPI AG, 1 (2020). https://doi.org/10.3390/antibiotics9030107
20. Karki, R. et al. In vitro antimicrobial synergy testing of extensively drug-resistant clinical isolates at an organ transplant center in nepal. *Infect. Drug Resist.* **14**, 1669–1677. https://doi.org/10.2147/IDR.S309531 (2021).

21. Almoudi, M. M. et al. Antibacterial effectiveness of different zinc salts on Streptococcus mutans and Streptococcus sobrinus: An in-vitro study. *Saudi Dent. J.* **35** (7), 883–890. https://doi.org/10.1016/j.sdentj.2023.07.003 (2023).
22. Eduvirgem, J. et al. Antimicrobial and Antibiofilm Activities of Desloratadine Against Multidrug-Resistant Acinetobacter Baumannii. *Future Microbiol.* **18** (1), 15–25. https://doi.org/10.2217/fmb-2022-0085 (2023).
23. Zuluaga, A. F. S. B. E. R. C. A. Z. A. X. A. M. V. O. Neutropenia induced in outbred mice by a simplified low-dose cyclophosphamide regimen: characterization and applicability to diverse experimental models of infectious diseases. *BMC Infect. Dis.* **6** (1), 55. https://doi.org/10.1186/1471-2334-6-55 (2006).
24. Canonica, G. W., Blaiss, M. & Antihistaminic Anti-Inflammatory, and Antiallergic Properties of the Nonsedating Second-Generation Antihistamine Desloratadine: a Review of the Evidence. *World Allergy Organ. J.* **4** (2), 47–53. https://doi.org/https://doi.org/10.1097/WOX.0b013e3182093e19 (2011).
25. Kiouri, D. P. et al. MULTIFUNCTIONAL ROLE OF ZINC IN HUMAN HEALTH: AN UPDATE. In: *EXCLI Journal*. *Leibniz Res. Centre Working Environ. Hum. Factors 2 Jan*. **22**, 809–827. https://doi.org/10.17179/excli2023-6335 (2023). Preprint.
26. Zou, D. Bakuchiol reduces the severity of Mycoplasma pneumoniae-induced pneumonia in mice by attenuating inflammatory responses. *Arab. J. Chem.* **16** (10). https://doi.org/10.1016/j.arabjc.2023.105172 (2023).
27. Alcock, B. P. et al. CARD 2023: expanded curation, support for machine learning, and resistome prediction at the Comprehensive Antibiotic Resistance Database. *Nucleic Acids Res.* **51** (1 D), D690–D699. https://doi.org/10.1093/nar/gkac920 (2023).
28. Ghahremanian, S. et al. Molecular dynamics simulation approach for discovering potential inhibitors against SARS-CoV-2: A structural review. In: *Journal of Molecular Liquids*, vol. 354. Preprint, Elsevier B.V., 15 May (2022). https://doi.org/10.1016/j.molliq.2022.118901
29. Sariyer, A. S. et al. Mutations in the proximal binding site and F-loop of AdeJ confer resistance to efflux pump inhibitors. *Antimicrob. Agents Chemother.* **69** (8). https://doi.org/10.1128/aac.00090-25 (2025).
30. Momin-Reza, M. et al. Evaluating the ciprofloxacin potentiation efficacy of repurposed drug flupentixol through efflux pump inhibition of pathogenic bacteria. *Sci. Rep.* **15** (1). https://doi.org/10.1038/s41598-025-24167-5 (2025).
31. Wang, Y., Zhou, Y. & Khan, F. I. Molecular Insights into Structural Dynamics and Binding Interactions of Selected Inhibitors Targeting SARS-CoV-2 Main Protease. *Int. J. Mol. Sci.* **25** (24). https://doi.org/10.3390/ijms252413482 (2024).
32. Islam, M. T. et al. In silico screening of naturally derived dietary compounds as potential butyrylcholinesterase inhibitors for Alzheimer's disease treatment. *Sci. Rep.* **15** (1). https://doi.org/10.1038/s41598-025-98092-y (2025).
33. Abouzied, A. S. et al. Structural and free energy landscape analysis for the discovery of antiviral compounds targeting the cap-binding domain of influenza polymerase PB2. *Sci. Rep.* **14** (1). https://doi.org/10.1038/s41598-024-69816-3 (2024).
34. Ahamad, S. et al. Insights into the structure and dynamics of SARS-CoV-2 spike glycoprotein double mutant L452R-E484Q. *3 Biotech.* **12** (4). https://doi.org/10.1007/s13205-022-03151-0 (2022).

35. Vareschi, S. et al. Sep. Antimicrobial efflux and biofilms: an interplay leading to emergent resistance evolution. In: *Trends in Microbiology*, no. 9. Preprint, Elsevier Ltd, 1 33.1018–32. (2025). https://doi.org/10.1016/j.tim.2025.04.012
36. Alav, I., Sutton, J. M. & Rahman, K. M. Role of bacterial efflux pumps in biofilm formation. *J. Antimicrob. Chemother.* **73** (8), 2003–2020. https://doi.org/10.1093/jac/dky042 (2018).
37. Jo, D. M. et al. Understanding the role of drug efflux pumps in biofilms and virulence properties: Multiple potential strategies controlling bacterial infections. *Int. J. Antimicrob. Agents*. **66** (5), 107584. https://doi.org/https://doi.org/10.1016/j.ijantimicag.2025.107584 (2025).
38. Baugh, S. et al. Inhibition of multidrug efflux as a strategy to prevent biofilm formation. *J. Antimicrob. Chemother.* **69** (3), 673–681. https://doi.org/10.1093/jac/dkt420 (2014).
39. Kaatz, G. W. et al. Phenothiazines and thioxanthenes inhibit multidrug efflux pump activity in Staphylococcus aureus. *Antimicrob. Agents Chemother.* **47** (2), 719–726. https://doi.org/10.1128/AAC.47.2.719-726.2003 (2003).
40. Szemerédi, N. et al. Overcoming Multidrug Resistance by Bacterial Efflux Pump Inhibitors in Clinical Escherichia coli Strains. *Antibiotics* **15** (3). https://doi.org/10.3390/antibiotics15030276 (2026).
41. BenchChem *Preliminary Investigation into the Antimicrobial Properties of Zinc Gluconate: A Technical Guide*. (2026). https://www.benchchem.com/product/b10779097#preliminary-investigation-into-zinc-gluconate-s-antimicrobial-properties (13 Apr. 2026, date last accessed).
42. Dreno, B. F. P. R. A. M. D. H. H. R. H. Effect of zinc gluconate on propionibacterium acnes resistance to erythromycin in patients with inflammatory acne: in vitro and in vivo study. In: *Eur J Dermatol*, vol. 15, no. 2. Taylor and Francis Ltd: Taylor and Francis Ltd, (2005).
43. Soleimani, M. et al. The effect of zinc nanoparticles inhibitor of efflux pumps NorA and NorB in clinical isolated of Staphylococcus aureus from skin infections. *Med. Biomedical J.* **1** (01), 40–52 (2024).
44. EUCAST. EUCAST Disk Diffusion Method for Antimicrobial Susceptibility Testing. (2025).
45. Shaikh, S. S., Bawazir, A. S., Yahya, B. A. & Phytochemical Histochemical and In Vitro Antimicrobial Study of Various Solvent Extracts of Costus speciosus (J. Koenig) Sm. and Costus pictus D. Don. *Turk. J. Pharm. Sci.* **19** (2), 145–152. https://doi.org/10.4274/tjps.galenos.2021.02058 (2022).
46. Faruqe, M. O. Modulating the antibacterial effect of the existing antibiotics along with repurposing drug metformin. *Arch. Microbiol.* **206** (4). https://doi.org/10.1007/s00203-024-03917-5 (2024).
47. Bergamini, G. et al. Mouse pneumonia model by Acinetobacter baumannii multidrug resistant strains: Comparison between intranasal inoculation, intratracheal instillation and oropharyngeal aspiration techniques. *PLoS One*. **16** (12 December). https://doi.org/10.1371/journal.pone.0260627 (2021).
48. Saperi, A. A., Lee, H. Y. & Abubakar, S. Induction of pneumonia in multidrug-resistant Acinetobacter baumannii infected immunocompetent BALB/c mice. *Trop. Biomed.* **42** (2), 155–161. https://doi.org/10.47665/tb.42.2.008 (2025).
49. Sattar, S. B. A. N. A. S. S. *Bacterial Pneumonia*. n.p.: StatPearls, (2024). https://www.ncbi.nlm.nih.gov/books/NBK513321/ (12 Apr. 2026, date last accessed).
50. Luo, H. et al. Pathological observations of lung inflammation after administration of IP-10 in influenza virus- and respiratory syncytial virus-infected mice. *Exp. Ther. Med.* **3** (1), 76–79. https://doi.org/10.3892/etm.2011.350 (2012).

51. Grant, J. R. et al. Proksee: In-depth characterization and visualization of bacterial genomes. *Nucleic Acids Res.* **51** (W1), W484–W492. https://doi.org/10.1093/nar/gkad326 (2023).
52. Guex, N. P. M. C. SWISS-MODEL and the Swiss-Pdb Viewer: an environment for comparative protein modeling. *Electrophoresis* **18**, 2714–2723 (1997).
53. Abraham, M. J. et al. High performance molecular simulations through multi-level parallelism from laptops to supercomputers. *SoftwareX* **GROMACS**, 19–25. https://doi.org/https://doi.org/10.1016/j.softx.2015.06.001 (2015).
54. Sajadi, F. & Rowley, C. Apr. The CHARMM36 Force Field for Lipids Can Be Used With More Accurate Water Models. Preprint, 13 (2018). https://doi.org/10.26434/chemrxiv.6137474.v1
55. Ke, Q. et al. Effects of thermostats/barostats on physical properties of liquids by molecular dynamics simulations. *J. Mol. Liq*. **365**, 120116. https://doi.org/https://doi.org/10.1016/j.molliq.2022.120116 (2022).
56. Tan, T. K. Practical t-test Power Analysis with R. *Practical Assess. Res. Evaluation*. **27**, 18. https://doi.org/doi.org/10.7275/mmna-sh25 (2022).

Figures

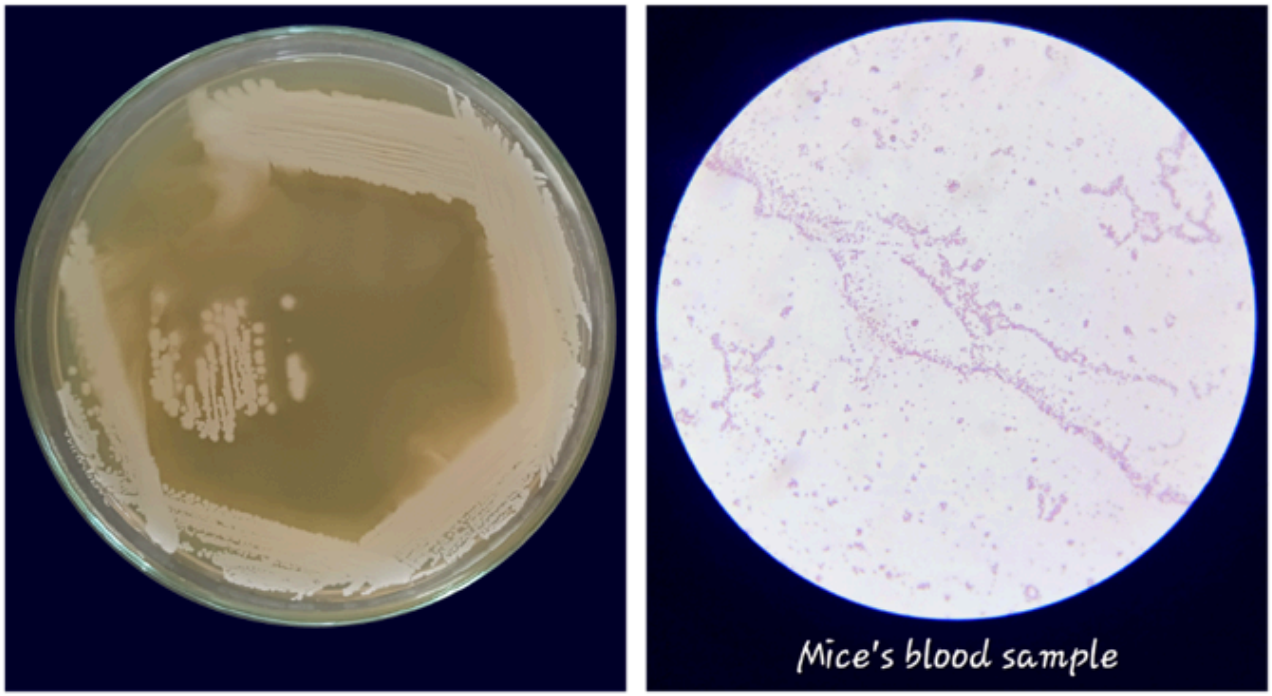

Figure 1

A) The culture of *Acinetobacter baumannii*-induced mice's sample; B) Color appearance of Gram-negative bacteria.

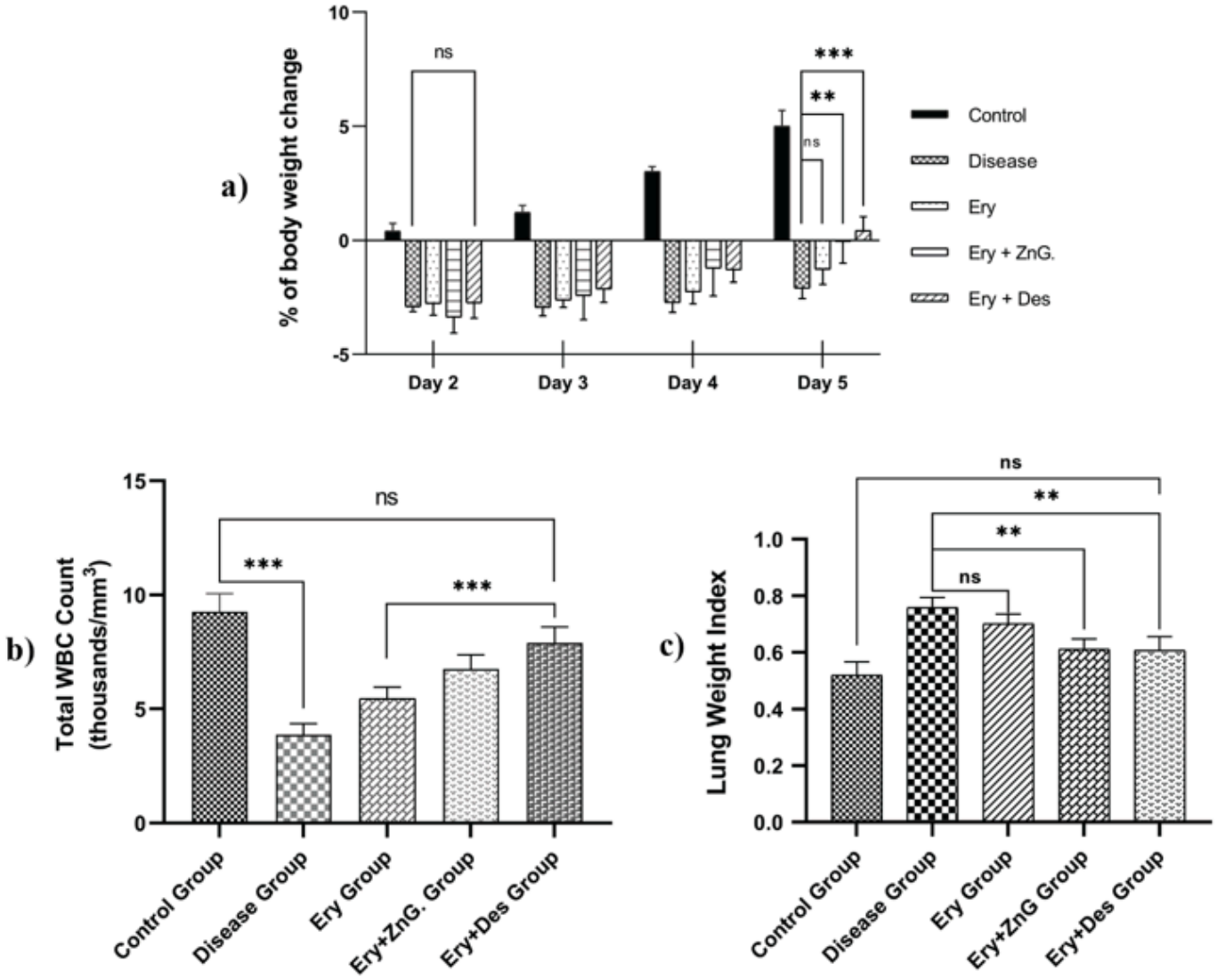

Figure 2

Outcomes of erythromycin and its combination with desloratadine and zinc gluconate on (a) Percentage of body weight change (b) total white blood cell levels, and (c) Lung weight index (LWI). The significant difference among the groups as established by an ordinary one-way ANOVA is shown by asterisks, here, *p < 0.05, **p < 0.01, ***p < 0.001

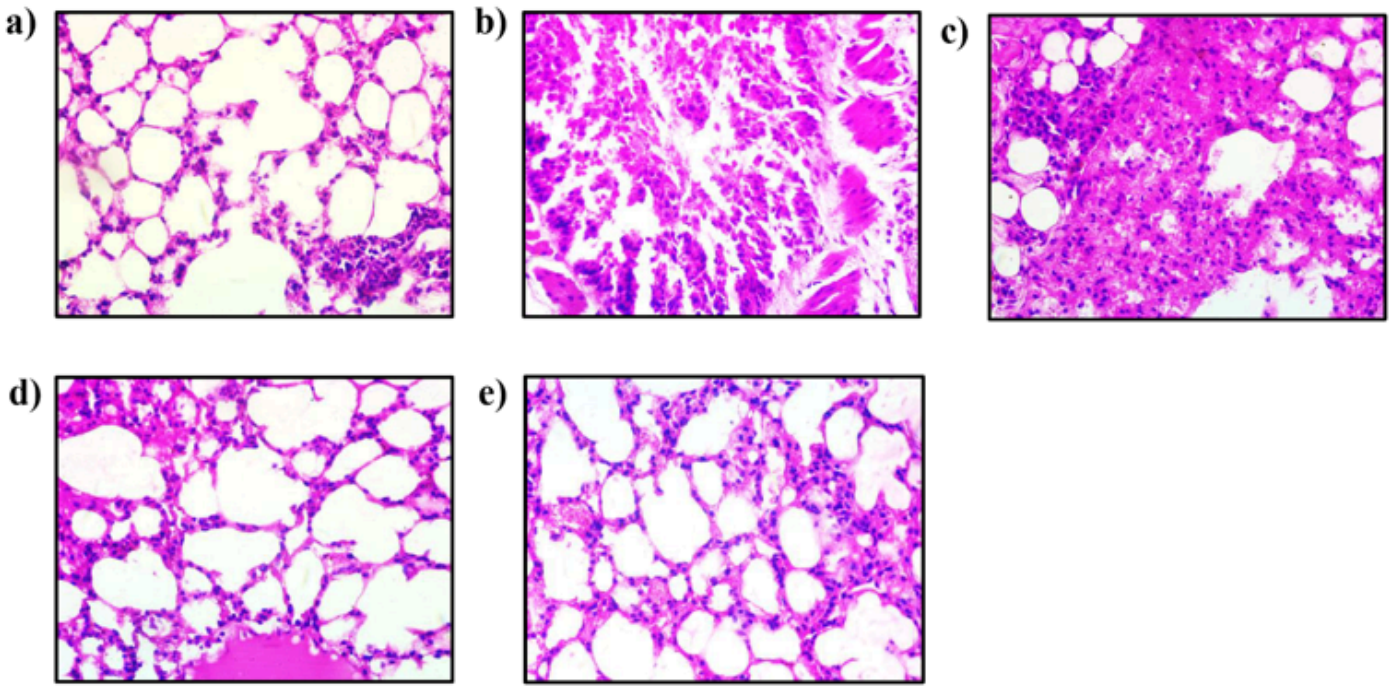

Figure 3

The preventive efficacy of the treatments was evaluated by histopathological examination of hematoxylin and eosin-stained lung sections under a microscope, where a) Normal, b) Disease, c) Erythromycin, d) Ery + ZnG, e) Ery + Des groups.

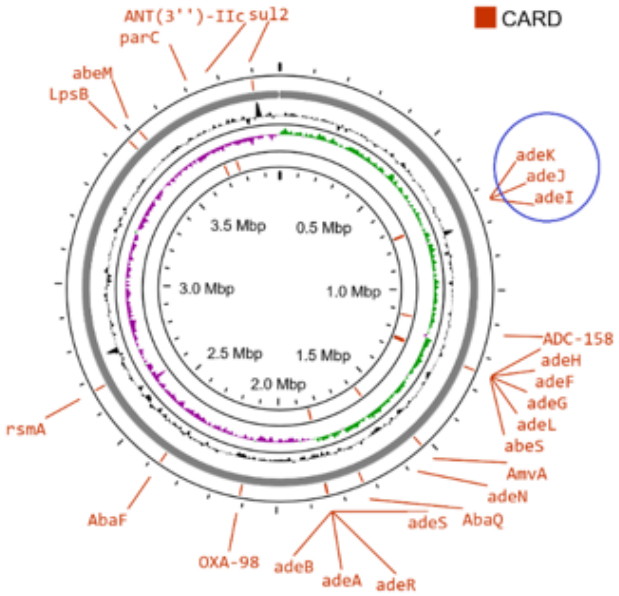

Figure 4

WGS MAP: CARD resistance genes of *Acinetobacter Baumannii* NCTC12156 genome assembly.

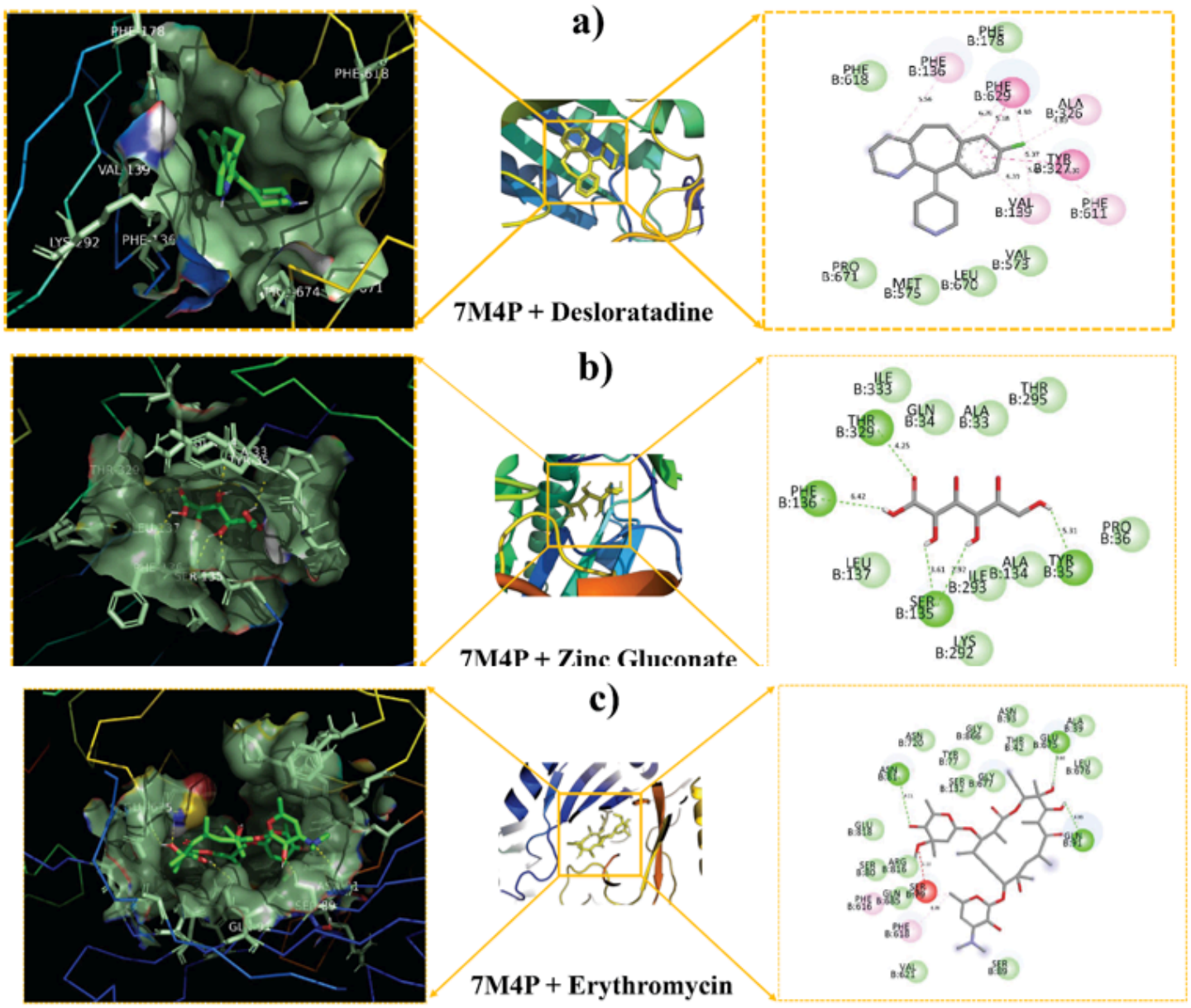

Figure 5

2D and 3D docking interaction of a) desloratadine, b) zinc gluconate, and c) control, erythromycin with target protein AdeJ (PDB ID: 7M4P).

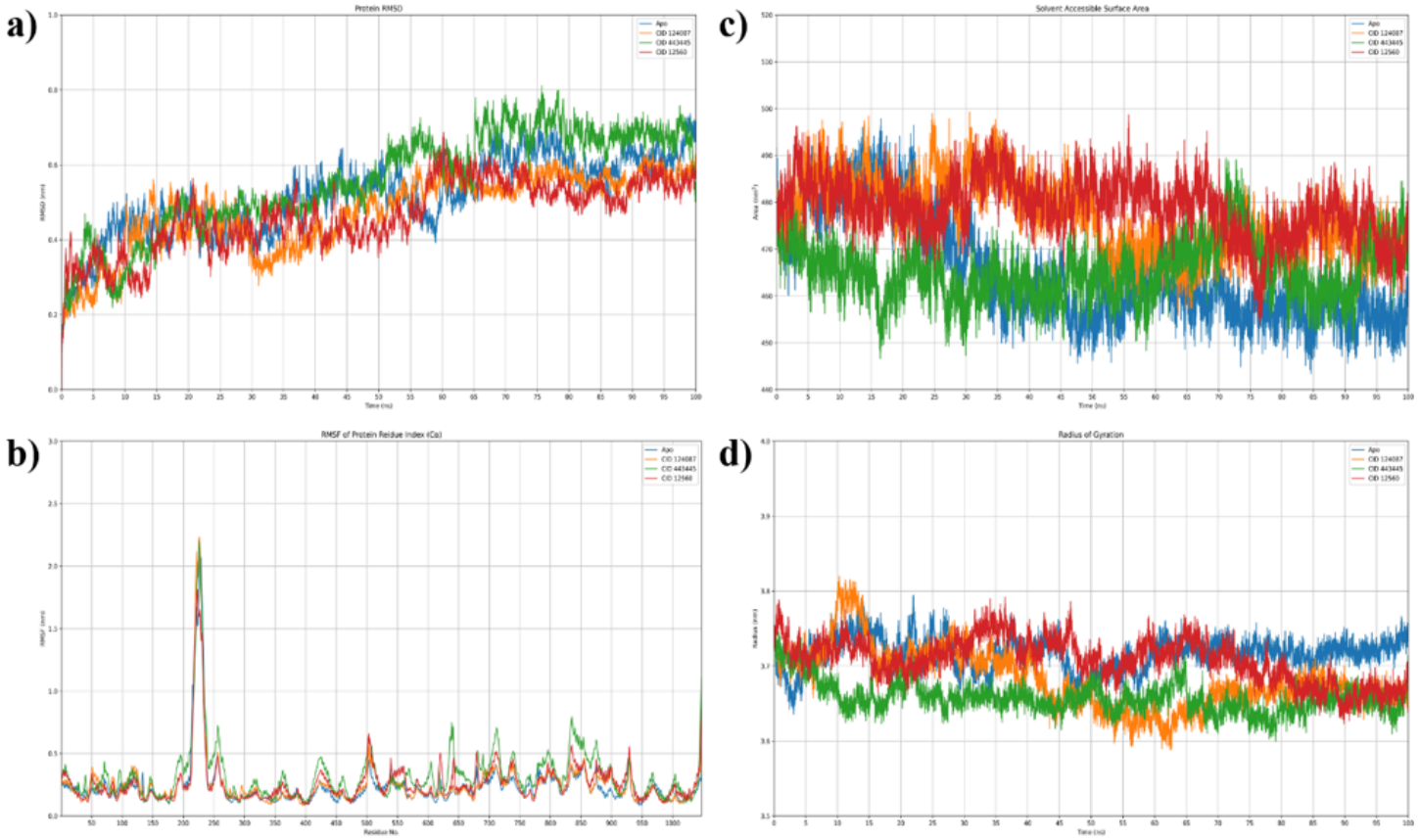

Figure 6

Graphical representation of **a)** RSMD, **b)** RMSF, **c)** SASA, and **d)**Radius of gyrase (Rg) analyses over the 100 ns simulation. The colors; orange, green and red represent for the protein (7M4P) complexed with desloratadine (CID 124087), zinc gluconate (CID 443445), and erythromycin (CID 12560) respectively whereas blue color indicates the apo-form of protein.

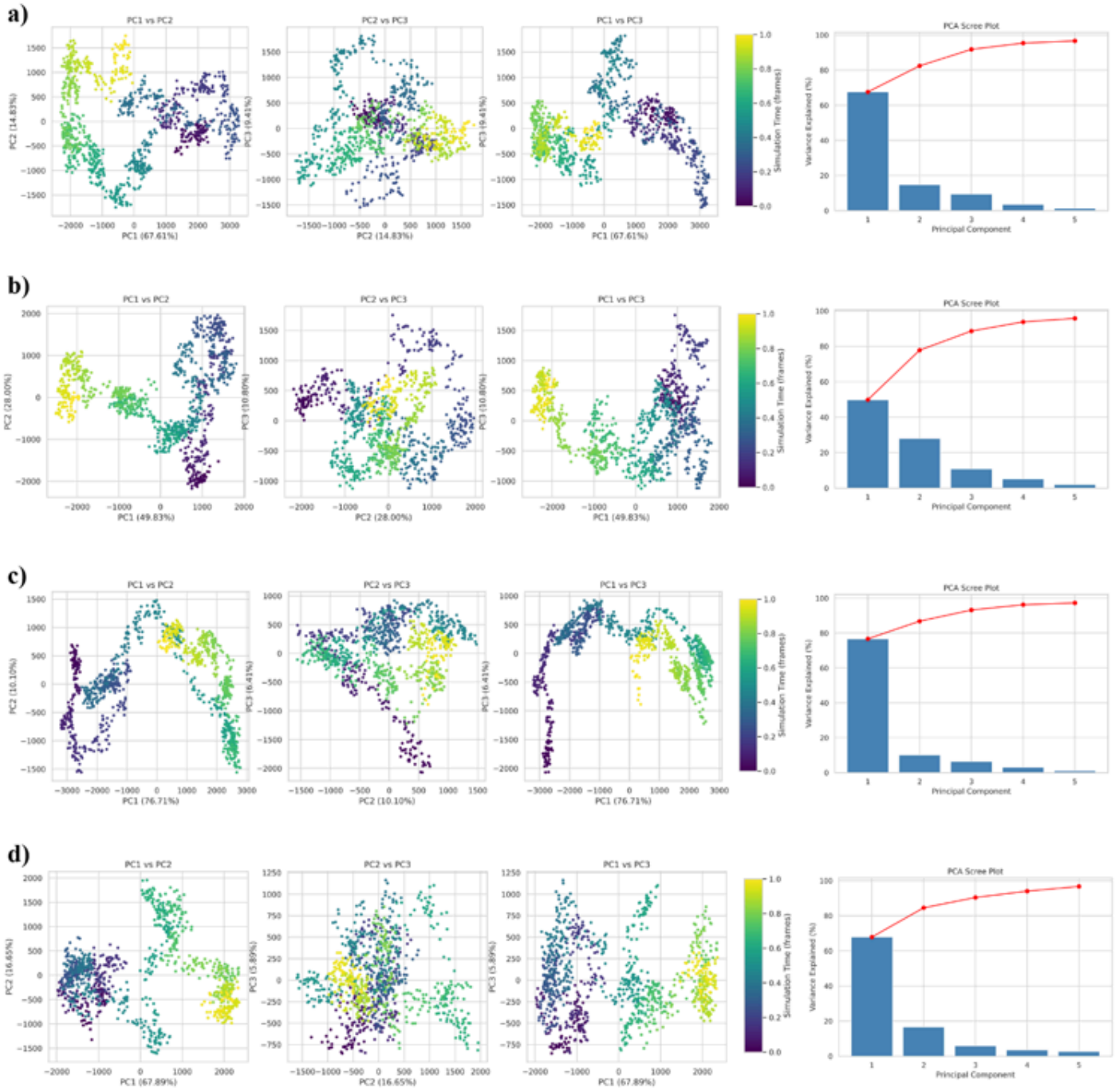

Figure 7

Figure 6. Represents the Principal component analysis (PCA) of **a)** Apo form, **b)** desloratadine (CID 124087)-7M4P complex , **c)** zinc gluconate (CID 443445)-7M4P complex, and **d)** erythromycin (CID 12560)-7M4P complex, where blue and yellow dots exhibit the simulation's representation of conformational modification of protein.

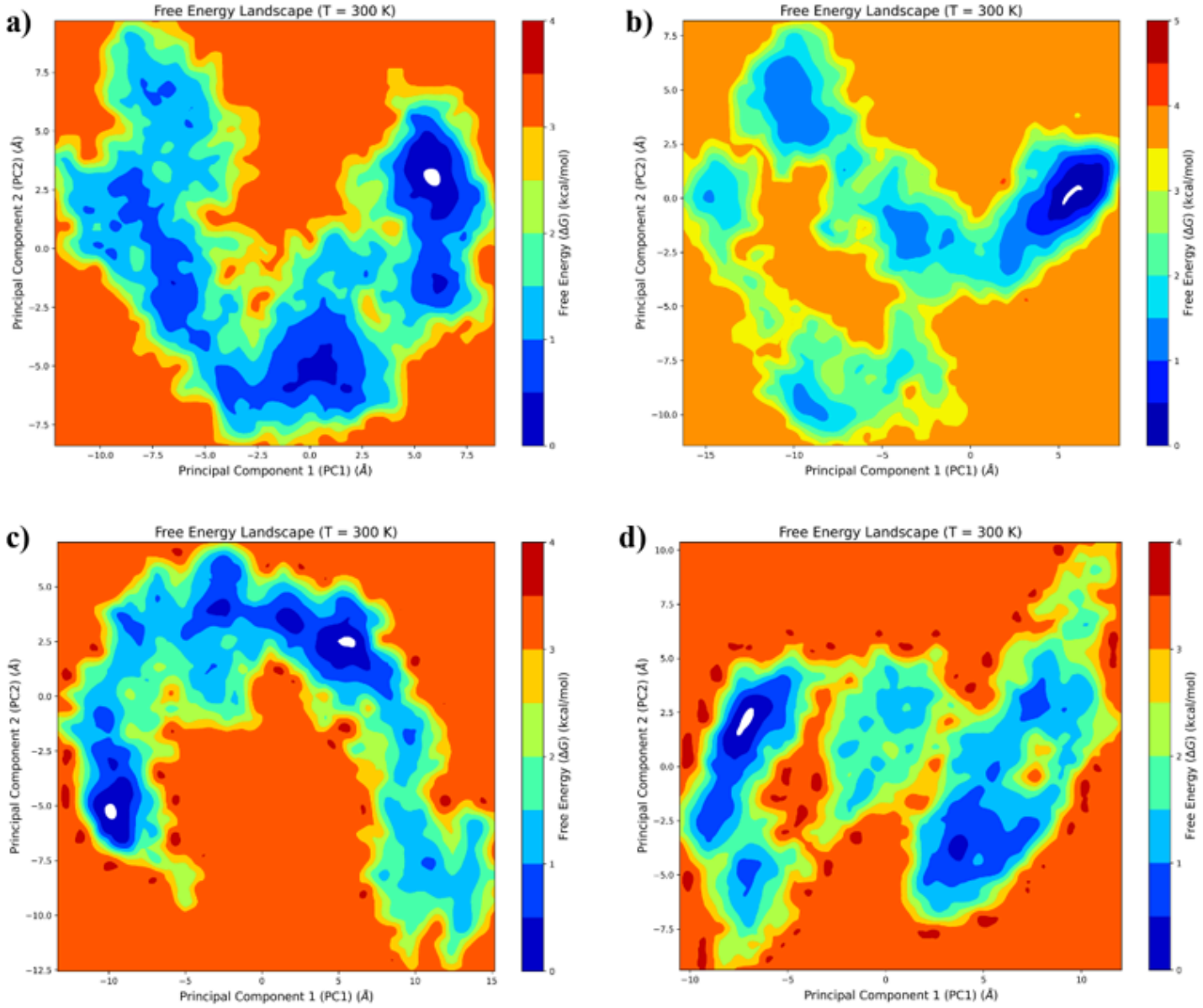

Figure 8

Figure 7. FEL analysis of **(8a)** Apo form, **(8b)** desloratadine (CID 124087)-7M4P complex , **(8c)** zinc gluconate (CID 443445)-7M4P complex, and **(8d)** erythromycin (CID 12560)-7M4P complex, where the energy decreases in the order of dark red < red < yellow < green < blue < violet.

Supplementary Files

This is a list of supplementary files associated with this preprint. Click to download.

- SupportingInformations.pdf